Brain Research 1817 (2023) 148496

Contents lists available at ScienceDirect

Brain Research

journal homepage: www.elsevier.com/locate/brainres

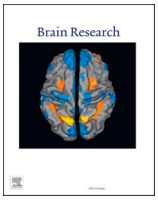

Short Report

Tight control of the APP-Mint1 interaction in regulating amyloid production

Shawna M. Henry [a,1], Sabrina A. Kistler [a,1], Gavin D. Lagani [a,1], Christian R.O. Bartling [b], Dennis Özcelik [b], Vita Sereikaite [b], Kristian Strømgaard [b], Uwe Beffert [a], Angela Ho [a,*]

[a] Department of Biology, Boston University, Boston, MA, USA
[b] Department of Drug Design and Pharmacology, University of Copenhagen, Copenhagen, Denmark

ARTICLE INFO

Keywords:
Mint1
APP
Amyloid
Alzheimer's disease

ABSTRACT

Generation of amyloid-β (Aβ) peptides through the proteolytic processing of the amyloid precursor protein (APP) is a pathogenic event in Alzheimer's disease (AD). APP is a transmembrane protein and endocytosis of APP mediated by the YENPTY motif is a key step in Aβ generation. Mints, a family of cytosolic adaptor proteins, directly bind to the YENPTY motif of APP and facilitate APP trafficking and processing. Here, we generated and examined two Mint1 mutants, Tyr633Ala of Mint1 (Mint1^{Y633A}) that enhanced APP binding, and Tyr549Ala and Phe610Ala mutant (Mint1$^{Y549A/F610A}$), that reduced APP binding. We investigated how perturbing the APP-Mint1 interaction through these Mint1 mutants alter APP and Mint1 cellular dynamics and Mint1's interaction with its other binding partners. We found that Mint1^{Y633A} increased binding affinity specifically for APP and presenilin1 (catalytic subunit of γ-secretase), that subsequently enhanced APP endocytosis in primary murine neurons. Conversely, Mint1$^{Y549A/F610A}$ exhibited reduced APP affinity and Aβ secretion. The effect of Mint1$^{Y549A/F610A}$ on Aβ release was greater compared to knocking down all three Mint proteins supporting the APP-Mint1 interaction is a critical factor in Aβ production. Altogether, this study highlights the potential of targeting the APP-Mint1 interaction as a therapeutic strategy for AD.

1. Introduction

Accumulation of amyloid-β (Aβ) peptides into insoluble plaques is a pathological hallmark of Alzheimer's disease (AD). Aβ is produced by the sequential proteolytic processing of the amyloid precursor protein (APP) by β- and γ- secretases (Selkoe and Hardy, 2016). In neurons, APP accumulates in the *trans*-Golgi complex before trafficking to the plasma membrane and subsequent internalization to endosomes initiate the amyloidogenic pathway, where APP is cleaved by β-secretase. The sorting signal that regulates APP endocytic processing is the conserved YENPTY sequence located in the cytoplasmic region of APP (Haass et al., 2012; Lai et al., 1995; Perez et al., 1999).

Mints (also known as APP binding family A, APBA) are a family of neuronal adaptor proteins that directly bind to the YENPTY motif of APP and regulate APP processing (Ho et al., 2008). Mints are encoded by three distinct genes: neuron-specific Mint1 and Mint2 and the ubiquitously expressed Mint3 (Okamoto and Sudhof, 1997). Mints consist of a divergent N-terminus and a conserved C-terminus that encodes a phosphotyrosine binding (PTB) domain, an α-helical linker (ARM) domain, and two tandem PDZ domains. Through the crystal structure of Mint1, we found the ARM domain adjacent to the PTB domain folds back, and sterically hinders APP binding (Matos et al., 2012). A single point mutation in Y633A of Mint1 in the ARM domain has been shown to relieve autoinhibition and increase APP binding. Conversely, mutations in the Mint2 PTB domain (Y459A and F520A) led to reduced APP binding and decreased Aβ generation (Bartling et al., 2021). However, the cellular mechanisms underlying how these Mint full-length mutants modify APP binding and Aβ generation is unclear.

Here we examined two full-length Mint1 mutants, Mint1^{Y633A} and Mint1$^{Y549A/F610A}$ (analogous to Y459 and F520 in Mint2), to determine the binding specificity to APP and Mint1 interacting partners. In addition, we examined the cellular mechanistic effects of Mint1 mutants in primary neurons. We found Mint1$^{Y549A/F610A}$ selectively decreased APP binding without interfering with Mint1 interacting proteins to decrease

* Corresponding author.
E-mail address: aho1@bu.edu (A. Ho).
[1] Co-first authors.

https://doi.org/10.1016/j.brainres.2023.148496
Received 15 November 2022; Received in revised form 17 July 2023; Accepted 20 July 2023
Available online 25 July 2023

APP endocytosis and Aβ production in neurons.

2. Results

2.1. Mint1 mutants exhibit differential binding affinities to APP and Mint1 interacting partners

To assess the ability of Mint1 to bind APP and other interacting partners, we produced two full-length GFP-tagged Mint1 mutants, GFP-Mint1^{Y633A} and GFP-Mint1$^{Y549A/F610A}$ to compare with GFP-Mint1^{WT}. We measured their ability to interact with the APP family of proteins including, APLP1 and APLP2 by co-transfecting with GFP-Mint1^{WT}, GFP-Mint1^{Y633A}, or GFP-Mint1$^{Y549A/F610A}$ in HEK293T cells. We performed a co-immunoprecipitation assay where we immunoprecipitated with GFP antibody and immunoblotted for Mint1 and APP. Both full-length GFP-tagged Mint1 mutants did not affect Mint1 levels compared to GFP-Mint1^{WT} (Fig. 1A, B, C). However, GFP-Mint1^{Y633A} enhanced APP binding by 767% compared to GFP-Mint1^{WT} (lane 7 compared to 6, Fig. 1A). Meanwhile, GFP-Mint1$^{Y549A/F610A}$ reduced APP binding by 82% compared to GFP-Mint1^{WT} (lane 8 compared to 6, Fig. 1A). Similarly, GFP-Mint1^{Y633A} enhanced Mint1 binding to APLP1 and APLP2 (Fig. 1B, C). Conversely, GFP- Mint1$^{Y549A/F610A}$ reduced binding to APLP1 and APLP2 (Fig. 1B, C).

We next determined whether the Mint1 mutants specifically altered binding to APP, and not to other Mint1 interacting partners. To test this, we quantified the interaction of Mint1^{WT} and Mint1 mutants with known interacting partners such as presenilin 1 (PS1), cell adhesion molecule neurexin (Nrxn 1), and voltage-gated calcium channel 2.2 (VGCC 2.2) using fluorescence polarization (FP) and analyzed peptides that were used in previous binding studies (Bartling et al., 2021; Jensen et al., 2018). We used recombinantly expressed Mint1 C-terminal constructs encompassing 453–839 amino acids that carried the Y549/F610A or Y633A mutations, and tested the 17-mer APP C-terminal peptide that encompassed the endocytic YENPTY motif. Based on the FP

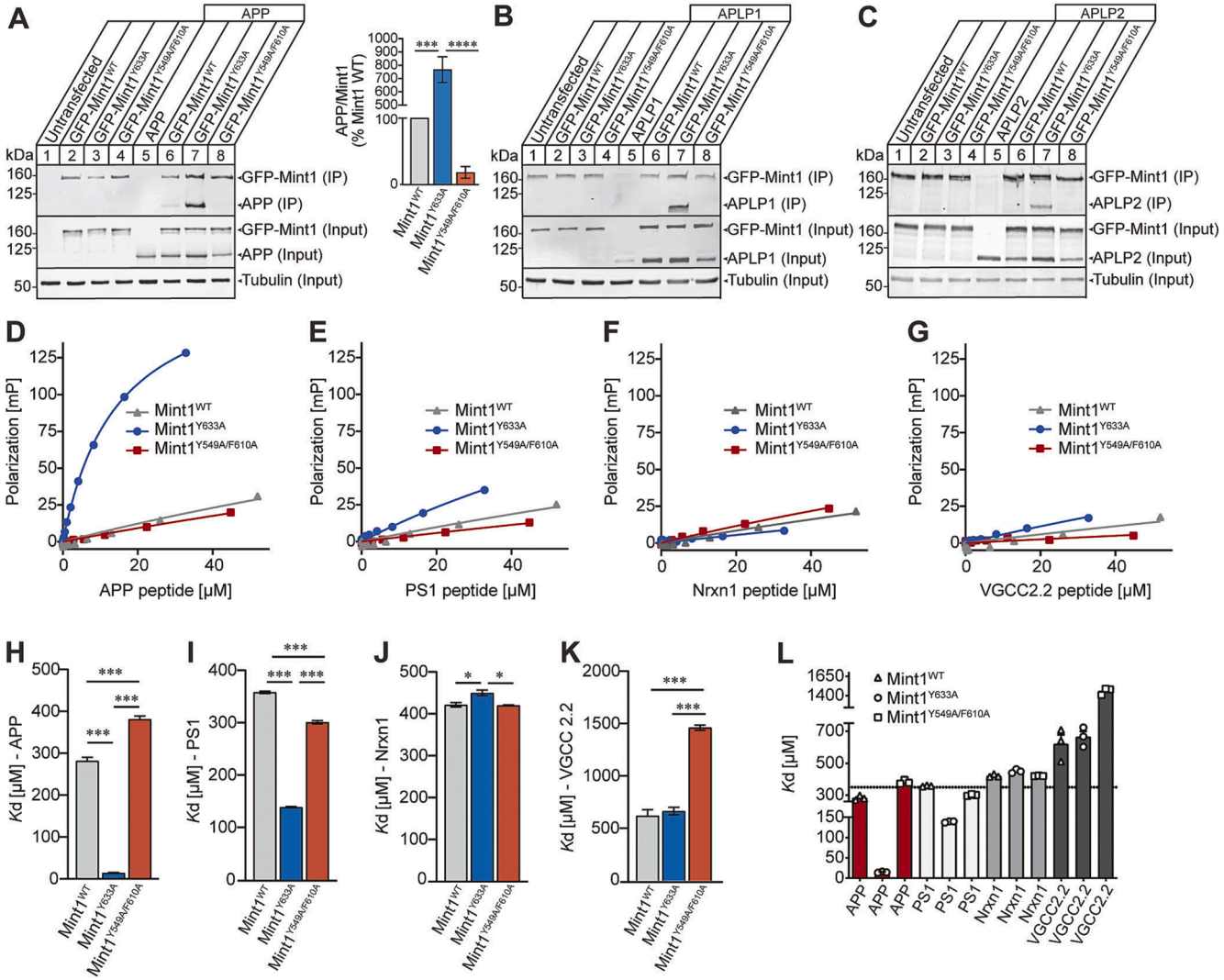

Fig. 1. Biochemical analysis of Mint1 mutants with APP family of proteins and interacting partners. (A-C) HEK293T cells were transfected GFP-Mint1^{WT}, GFP-Mint1^{Y633A}, or GFP-Mint1$^{Y549A/F610A}$ alone or co-transfected with APP, APLP1 or APLP2. Cell lysates were immunoprecipitated (IP) with GFP antibody and immunoblotted for APP, APLP1, APLP2, GFP, and tubulin. The amount of immunoprecipitate was normalized to the amount of precipitated Mint1 and shown as percent Mint1^{WT} control. Data are expressed as the mean ± SEM (n = 4 independent experiments). Statistical significance was evaluated using one-way ANOVA with Sidak's multiple comparison test, ***p = 0.00012 and **** p = 0.00009. (D-G) Fluorescence polarization (FP) saturation curves of the binding of APP peptide (D), PS1 (E), Nrxn1 (F), VGCC2.2 to recombinantly expressed Mint1^{WT}, Mint1^{Y633A}, or Mint1$^{Y549A/F610A}$ mutations. (H-K) Affinity fold-change to APP peptide (H), PS1 (I), Nrxn1 (J), VGCC2.2 (K) toward Mint1^{WT}, Mint1^{Y633A}, or Mint1$^{Y549A/F610A}$ mutations obtained in a FP assay. (L) Summary comparison of fold change for APP and Mint1 interacting partners toward Mint1^{WT} and mutants (n = 1 independent experiment with 3 biological replicates). Statistical significance was evaluated using one-way ANOVA with Sidak's multiple comparison test, *p < 0.05 and ***p < 0.0001.

saturation curves of the APP peptide to Mint1 mutants, Mint1^{Y633A} showed enhanced binding affinity with K_d of 14.5 ± 0.74 μM, a 19-fold increase compared to Mint1^{WT} (K_d = 282 ± 8.3 μM) (Fig. 1D, H). Mint1$^{Y549A/F610A}$ exhibited a lower affinity to APP peptide (K_d = 382 ± 12.5 μM) compared to Mint1^{WT}. Interestingly, we found Mint1^{Y633A} preferentially bound PS1 peptide with higher affinity (K_d = 138.8 ± 1.02 μM), at least a 2-fold increase compared to Mint1^{WT} (K_d = 358 ± 2.0 μM), and Mint1$^{Y549A/F610A}$ (K_d = 301 ± 3.0 μM) (Fig. 1E, I). However, the binding affinity of Mint1^{Y633A} to PS1 peptide was not as strong compared to APP peptide. Based on the FP saturation curves for Nrxn1 and VGCC2.2 peptides to Mint1^{WT} and Mint1 mutants, the binding affinity was much lower with a K_d range of 420–664 μM (Fig. 1F, G, J, K). We observed the weakest affinity between Mint1$^{Y549A/F610A}$ and the VGCC2.2 peptide (K_d = 1461 ± 25.2 μM) compared to Mint1^{WT} (K_d = 619 ± 57.9 μM) (Fig. 1K). Overall, we found Mint1^{Y633A} enhanced binding to both APP and PS1 and Mint1$^{Y549A/F610A}$ mutant exhibited a reduction in APP binding.

2.2. *Mint1 mutants alters Golgi and APP co-localization in primary neurons*

To determine whether the Mint1 mutants affect Mint1 localization in neurons, we cultured primary neurons from mice that lacked endogenous Mint1, and infected with lentivirus that expressed GFP-Mint1^{WT}, GFP-Mint1^{Y633A}, or GFP-Mint1$^{Y549A/F610A}$ at DIV 2. Since previous studies have shown that Mint proteins localize to the Golgi apparatus (Biederer et al., 2002), we immuno-labeled for Mint1 and the Golgi marker GM130 at DIV 10. Both GFP-Mint1^{WT} and GFP-Mint1^{Y633A} overlapped with GM130, with slightly more co-localization between GFP-Mint1^{Y633A} and GM130 compared to GFP-Mint^{WT} (Fig. 2A, B). Meanwhile, we observed diffuse labeling of GFP-Mint1$^{Y549A/F610A}$ and decreased co-localization with GM130. We also quantitatively assessed Golgi morphology that has been linked to different cellular processes (Makhoul et al., 2019), with the Golgi defined as "condensed" when it appeared compact and nearly circular in shape, and "ribbon" when the Golgi is extended with multiple cisternae. We found neurons infected with GFP-Mint1^{Y633A} tend to have more "condensed" Golgi morphology compared to GFP-Mint1^{WT} and GFP- Mint1$^{Y549A/F610A}$ (Fig. 2C).

We next examined whether Mint1 mutants altered co-localization with APP by immuno-labeling for Mint1 and APP. Quantitative analysis of confocal images showed GFP-Mint1^{WT} and GFP-Mint1^{Y633A} exhibited 43% and 38% higher co-localization with APP in both soma and processes compared to GFP- Mint1$^{Y549A/F610A}$, respectively (Fig. 2D, E, F). We also examined GFP-Mint1^{WT} and mutant Mint1 localization to synapses and did not observe any changes with presynaptic marker synapsin (Fig. 2G, H, I). These results suggest that the APP-Mint1 interaction is important for the localization of Mint1 to the Golgi which might be important to direct distinct cellular processes such as APP distribution across neurons.

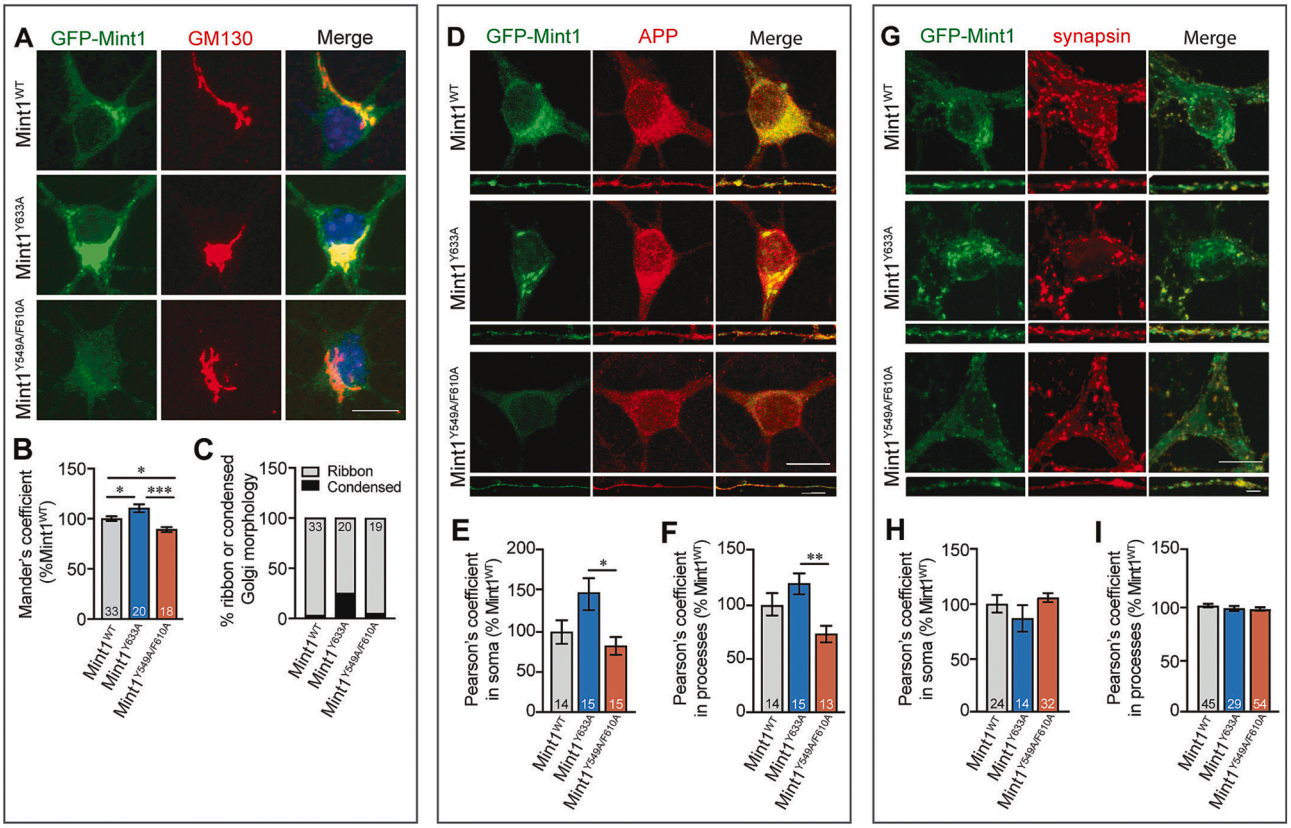

Fig. 2. Cellular localization of Mint1 mutants in primary neurons. (A) Primary murine neurons that lacked endogenous Mint1 and infected with GFP-Mint1^{WT}, GFP-Mint1^{Y633A}, or GFP-Mint1$^{Y549A/F610A}$ were immunolabeled with GFP and *cis*-Golgi marker GM130. Representative images show GFP-Mint1 (green) and Golgi staining (red). Scale bar = 10 μm. (B) Co-localization of GFP-Mint1 with GM130 was quantified. (C) Percentage of neurons exhibiting a ribbon or condensed Golgi phenotype. Same neurons as analyzed in panel B. (D) Representative images show GFP-Mint1 (green) and APP staining (red). Scale bar for soma = 10 μm and processes = 5 μm. (E-F) Co-localization of GFP-Mint1 with APP was quantified in soma and processes. (G) Representative images show GFP-Mint1 (green) and synapsin staining (red). Scale bar for soma = 10 μm and processes = 5 μm. (H-I) Co-localization of GFP-Mint1 with synapsin was quantified in soma and processes. Data are expressed as the mean ± SEM (n = 1 independent experiment, number at the bottom of each bar represents number of neurons analyzed from 3 to 4 coverslips per condition). Statistical significance was evaluated using one-way ANOVA with Sidak's multiple comparison test, *p ≤ 0.05, **p ≤ 0.01, ***p ≤ 0.001.

2.3. Mint1 mutants alter APP endocytosis and Aβ production in primary neurons

Activity-dependent APP endocytosis is a critical step in Aβ production (Cirrito et al., 2008; Das et al., 2013), and we have previously shown Mints are necessary for regulating activity-induced APP endocytosis and Aβ production (Sullivan et al., 2014). To examine whether Mint1 mutants alter APP endocytosis, we cultured neurons from homozygous triple-floxed conditional Mint mice. At DIV 2, neurons were infected with lentiviral *Cre* recombinase to knockdown all three Mint proteins, and rescued with either GFP-Mint1^{WT}, GFP-Mint1^{Y633A}, or GFP- Mint1$^{Y549A/F610A}$ lentivirus. Neuronal lysates collected at DIV 15 showed efficient knockdown for all three Mint proteins following *Cre* recombinase infection (lanes 3–10, Fig. 3A), whereas neurons infected with inactive *Cre* recombinase (Δ*Cre*) retain endogenous Mint expression (lanes 1–2, Fig. 3A). Expression of GFP-Mint1^{WT}, GFP-Mint1^{Y633A}, or GFP- Mint1$^{Y549A/F610A}$ lentivirus was comparable to endogenous Mint protein levels (lanes 5–10, Fig. 3A). In addition, we did not observe any changes in expression levels for APP, proteolytic products such as APP C-terminal fragments (CTFs) or soluble APP secretion (Fig. 3B, C).

To stimulate activity-induced APP endocytosis, neurons were treated with 25 μM glutamate for 15 min, and live-cell endocytosis for APP was

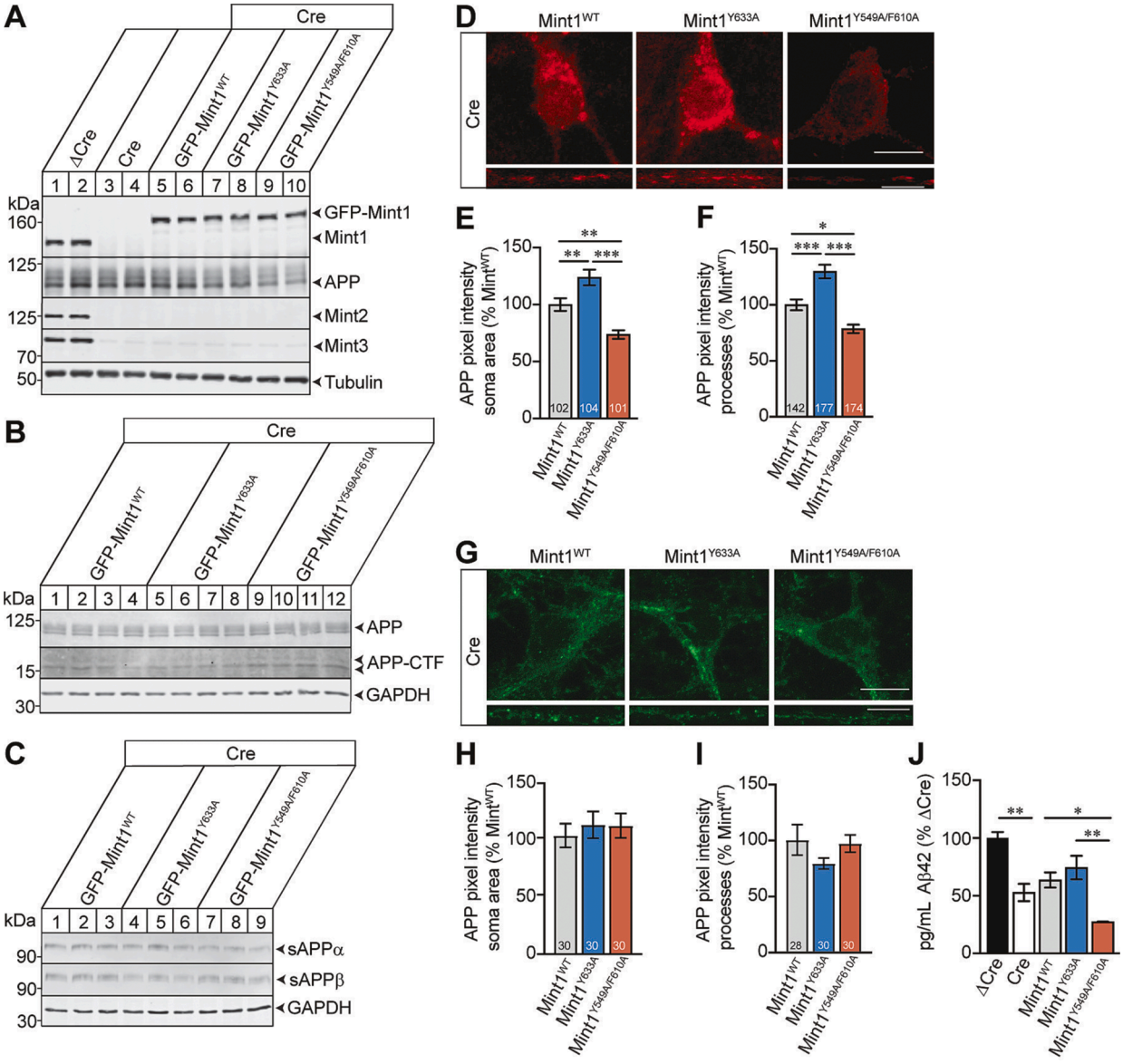

Fig. 3. Mint1 mutants alter APP endocytosis and Aβ production in primary neurons. Mint triple-floxed neurons were infected with inactive lentiviral *Cre* recombinase (*ΔCre*) or active *Cre* recombinase to knockdown Mints 1–3 and rescued with GFP-Mint1^{WT}, GFP-Mint1^{Y633A}, or GFP- Mint1$^{Y549A/F610A}$ lentivirus. (A) Representative immunoblot analysis of neuronal lysates immunoblotted for GFP, individual Mint proteins, APP and tubulin serves as a loading control. (B) Representative immunoblots of neuronal lysates immunoblotted for APP, APP-CTF and GAPDH as a loading control. (C) Representative immunoblots of neuronal lysates immunoblotted for sAPPα, sAPPβ and GAPDH. (D) Representative images showing internalized APP (red) in both the soma (top) and processes (bottom). Scale bars: soma = 10 μm; process = 5 μm. (E-F) Quantification of the amount of internalized APP using corrected total cell fluorescence in the neuronal soma and processes, expressed as percent Mint1^{WT}. (G) Representative images showing cell surface APP (green) in both the soma (top) and processes (bottom). (H-I) Quantification of the amount of cell surface APP using corrected total cell fluorescence in the neuronal soma and processes, expressed as percent Mint1^{WT}. Data are expressed as the mean ± SEM (n = 1–2 independent experiment, number at the bottom of each bar represents number of neurons analyzed). (J) Aβ42 ELISA quantification of conditioned media from neurons cultured from Mint triple-floxed carrying the human APPswe/PS1ΔE9 transgene. Data were normalized to *ΔCre* control, and expressed as the mean ± SEM (n = 1 independent experiment with 3 biological replicates). Statistical significance was evaluated using one-way ANOVA with Sidak's multiple comparison test, *p ≤ 0.05, **p ≤ 0.01, ***p ≤ 0.001.

performed at DIV 15. GFP-Mint1^{Y633A} induced a ~ 24% and 30% increase in internalized APP in the soma and processes compared to GFP-Mint1^{WT}, respectively (Fig. 3D, E, F). In contrast, neurons infected with GFP-Mint1$^{Y549A/F610A}$ exhibited a ~ 27% and 22% decrease in APP endocytosis in the soma and processes compared to GFP-Mint1^{WT}, respectively. Cell surface APP staining showed no difference between GFP-Mint1^{WT} and Mint1 mutants indicating that Mint1 mutants alter activity-induced APP endocytosis (Fig. 3G, H, I).

We next examined whether the changes in APP endocytosis affects Aβ production. We quantified Aβ42 levels released from primary neurons cultured from a mouse line that is homozygous floxed for all three *Mint* genes carrying the APPswe/PS1ΔE9 transgene that produces human Aβ42. Mint knockout neurons (*Cre*) exhibited a 44% decrease in Aβ42 production compared to neurons expressing Mints (Δ*Cre*), supporting our previous findings (Fig. 3J) (Ho et al., 2008, Matos et al., 2012, Chaufty et al., 2012; Sullivan et al., 2014). GFP-Mint1$^{Y549A/F610A}$ showed a robust 62.6% decrease in Aβ42 production compared to neurons expressing Mints (Δ*Cre*) and was significantly lower than the Mint1^{WT} and Mint1^{Y633A} rescue conditions suggesting the APP-Mint1 interaction is a critical factor in Aβ production. Neurons infected with GFP-Mint1^{WT} did not fully rescue the knockout phenotype which is likely due to the native autoinhibited state of Mint1 hindering its binding to APP.

3. Discussion

Here, we characterized two Mint1 mutants, Mint1^{Y633A} and Mint1$^{Y549A/F610A}$ that bind to APP with high and low affinity, respectively. We showed Mint1^{Y633A} exhibits increased PS1 binding compared to Mint1^{WT} supporting a mechanism whereby Mint1 promotes both APP and PS1 binding to enhance endocytic APP trafficking and processing. We found the low affinity Mint1$^{Y549A/F610A}$ mutant that targets two amino acids in the PTB domain reduced APP, APLP1 and APLP2 binding compared to Mint1^{WT} without affecting other Mint1 interacting partners such as PS1 and Nrxn1. Notably, Mint1$^{Y549A/F610A}$ exhibited a two-fold decrease affinity to VGCC2.2 as compared to Mint1^{WT}. However, these low-affinity interactions may not be physiologically relevant.

Mints typically localize predominantly to the Golgi and synapse in primary neurons (Biederer et al., 2002; Okamoto et al., 2000). We found Mint1^{Y633A} exhibited increased colocalization with the Golgi. In contrast, Mint1$^{Y549A/F610A}$ staining was more diffuse, with loss of colocalization with GM130, suggesting Mint1′s Golgi localization may be dependent on its interaction with APP. This is supported by previous work which showed Mint3 was recruited to the Golgi in an APP-dependent manner in Hela cells (Caster and Kahn, 2013). Further studies in *Drosophila* showed that Mints function at the Golgi to control polarized trafficking of axonal membrane proteins including APP (Gross et al., 2013). Considering Mint1$^{Y549A/F610A}$ loses its colocalization with GM130, this may perturb APP trafficking from the Golgi. Since the Golgi has been implicated as a site for APP processing (Fourriere and Gleeson, 2021), and alterations in Golgi morphology are a preclinical feature that occurs before AD-associated neurodegeneration (Dal Canto, 1996; Stieber et al., 1996), it is possible that Mints could be involved in APP processing at the Golgi. Altered APP processing at the Golgi might underlie the observed phenotype where Mint1^{Y633A} expressing neurons showed a greater number of neurons with a condensed Golgi morphology compared to Mint1^{WT} and Mint1$^{Y459A/F520A}$ mutant.

Lastly, neurons expressing Mint1$^{Y549A/F610A}$ showed a decrease in APP endocytosis and Aβ release when compared to both Mint1^{WT} and Mint1^{Y633A}. The effect of Mint1$^{Y549A/F610A}$ on Aβ production was greater than the effect produced by knocking down all three Mint proteins. This suggests that perturbing the APP-Mint1 interaction specifically at Y549 and F610 in Mint1 may provide a more selective and preferable alternative to regulate Aβ production without disrupting adaptor protein function with such a complex protein–protein interaction network.

4. Conclusion

We examined the biochemical and cellular dynamics of the APP-Mint1 interaction using two Mint1 mutants that bind APP high affinity (Mint1^{Y633A}) or low affinity (Mint1$^{Y549A/F610A}$). These Mint1 mutants exhibited profound alterations in cellular localization, APP endocytosis, and Aβ production, supporting the facilitative role of Mint1 in mediating APP trafficking and processing.

5. Experimental procedure

5.1. Plasmids

pEGFP-Mint1 was derived from *Rattus norvegicus* cDNA (NCBI NP_113967.1), and the pCMV5-APP695 construct was derived from *Homo sapiens* (NCBI NP_958817.1). To generate the rat pEGFP-Mint1^{Y633A} mutation, site-directed mutagenesis was performed with primer set: SMH1607 forward GAAGACCTGAGCCAGAAGGAG*GC*AAGCGACCT GCTCAACACCCAG and SMH1608 reverse CTGGGTGTTGAGCAGGTC GCT*TGC*CTCCTTCTGGCTCAGGTCTTC. To generate the rat pEGFP-Mint1$^{Y549A/F610A}$ mutation, we first mutated F610A mutation using primer set: SMH1721 forward, CAGTCCATCGGGCAGGCC*GC*CAGCGTT GCATACCAGGAG and SMG1722 reverse CTCCTGGTATGCAACGCTG*GC* GGCCTGCCCGATGGACTG. We then consecutively mutated the Y549A mutation using primer set: SMH1747 forward, GACCATTTCC*GC*CATCG CAGACATTG and SMH1748 reverse CTCAGAGGGTGGTCCATC. Subsequent pEGFP plasmids were subcloned into the lentiviral pFUW vector and all plasmids were fully sequenced.

5.2. Co-immunoprecipitation in HEK293T cells

HEK293T cells were lysed in 10 mM Tris HCl pH 8.0, 150 mM NaCl, 1 mM EDTA pH 8.0, and 1% Triton X-100, supplemented with protease and phosphatase inhibitors. The cell lysate was sonicated, incubated for 30 min at 4 °C and centrifuged at 21,130 *g*. Protein extracts were incubated with the precipitating antibody, followed by pre-equilibrated protein A or G Ultralink beads (Thermo Scientific). Precipitated proteins were eluted by boiling for 10 min in 2X sample reducing buffer and resolved by SDS-PAGE and subjected to Western blot analysis.

5.3. Primary murine neurons and lentiviral production

Primary neuronal cultures were prepared using either Mint mouse line that is *Mint1* and *Mint3* double knockout with floxed *Mint2* (*Mint1*$^{-/-}$*; fMint2/fMint2;Mint3*$^{-/-}$), Mint triple-floxed mouse line that is homozygous floxed for all three *Mint* genes or Mint triple-floxed mouse line carrying the human APPswe/PS1ΔE9 transgene (Jackson Laboratory, #004462) that was used for Aβ42 analysis. Briefly, newborn brain tissue was trypsinized, triturated, and plated onto either Matrigel coated glass coverslips or wells as previously described (Ho et al., 2008). Recombinant lentiviruses were produced by transfecting HEK293T cells with pRSV-REV, pMDLg/pRRE, and pCMV-VSVG with the addition of a shuttle vector encoding the gene of interest (pFUW). The media was changed to neuronal growth media 24 h after transfection and the conditioned media was collected, spun at 1,000 *g*, and filtered using a 0.45 μM filter.

5.4. Immunocytochemistry and image analysis

Neurons were fixed with 4% paraformaldehyde (Electron Microscopy Sciences), permeabilized and blocked in 10% goat serum (Invitrogen) and 0.1% saponin (Sigma) in PBS. Neurons were incubated with primary antibodies in blocking buffer at 4 °C overnight. For surface-expressed APP, neurons were fixed and labeled with anti-APP antibodies without detergent permeabilization. Neurons were washed with PBS and incubated with a secondary antibody conjugated to an Alexa

Fluor® (Invitrogen). Coverslips were mounted using ProLong Gold Antifade Mountant with DAPI (Invitrogen) and imaged using Z-stacks with a Carl Zeiss LSM 700 confocal microscope. Corrected total cell fluorescence of maximum intensity projections was acquired using FIJI (NIH). Co-localization was quantified using IMARIS or NIH Image J software (Oxford Instruments). Experimenters are blind to conditions during data acquisition and analysis.

5.5. Live-cell APP endocytosis assay

Live hippocampal cultures were incubated with mouse anti-APP 22C11, 1:500 (EMD Millipore) diluted in conditioned neuronal media for 15 min as previously described (Chaufty et al., 2012). Neurons were washed to remove any unbound antibodies. Next, neurons were treated with 25 μM glutamate for 15 min at 37 °C, and fixed with 4% paraformaldehyde. Any remaining APP antibodies were quenched with a non-fluorescent goat anti-mouse secondary antibody conjugated to horseradish peroxidase (Cell Signaling). Neurons were permeabilized with 10% goat serum and 0.3% Triton-X-100, followed by incubation with goat anti-mouse Alexa Fluor® 546 (Fisher Scientific).

5.6. Aβ42 ELISA

Conditioned neuronal media was diluted and handled according to the protocol of the Human Aβ42 Ultrasensitive ELISA Kit (Invitrogen).

5.7. Fluorescence polarization

All experiments were conducted in 150 or 500 mM NaCl, 25 mM HEPES, 1% bovine serum albumin, pH 7.4 at 25 °C. Fluorescence was measured at excitation/emission wavelength at 530/580 nm. The instrumental Z-factor was adjusted to maximum fluorescence and the G-factor was calibrated to give an initial milli-polarization at 20. Fluorescence polarization assays were performed as saturation experiments using TAMRA-APP17-mer [(TAMRA)-NNG-QNGYENPTYKFFEQMQN], TAMRA-PS1-10mer [(TAMRA)-NNG-QLAFHQFYI]; TAMRA-Nrxn1-10mer [(TAMRA)-NNG-KKNKDKEYYV]; TAMRA-VGCC2.2-20mer [(TAMRA)-NNG-LSSGGRARHSYHHPDQDHWC] at a concentration of 50 nM. The binding affinities were determined using a Safire plate reader (Tecan).

5.8. Antibodies

APP (N-terminus, EMD Millipore MAB348), APP (C-terminus, Sigma A8717), sAPPα (IBL 11088), sAPPβ (IBL 18957), APLP1 (T2263, Dr. Thomas Südhof), APLP2 (T2264, Dr. Thomas Südhof), GFP (Synaptic Systems 132002), GM130 (BD Biosciences 610822), Mint1 (P730, Dr. Thomas Südhof), Mint2 (Sigma M3319), Mint3 (Thermo-Scientific PA1-072), Synapsin (P610, Dr. Thomas Südhof) and tubulin (Cell Signaling 3873S).

5.9. Statistical analysis

All statistical analyses were performed using Prism 9 software (GraphPad). To determine statistical significance, we used one-way analysis of variance (ANOVA) coupled with either Sidak's or Dunnett's multiple comparisons test. All graphs depict mean ± standard error of the mean (SEM).

Funding

This work was supported by NIH R01 AG044499 (A. H.); R21 AG072433 (A.H.); and the Harold and Margaret Southerland Alzheimer's Research Fund.

Declaration of Competing Interest

The authors declare that they have no known competing financial interests or personal relationships that could have appeared to influence the work reported in this paper.

Data availability

Data will be made available on request.

References

Bartling, C.R.O., Jensen, T.M.T., Henry, S.M., Colliander, A.L., Sereikaite, V., Wenzler, M., Jain, P., Maric, H.M., Harpsoe, K., Pedersen, S.W., Clemmensen, L.S., Haugaard-Kedstrom, L.M., Gloriam, D.E., Ho, A., Stromgaard, K., 2021. Targeting the APP-Mint2 protein-protein interaction with a peptide-based inhibitor reduces amyloid-beta formation. J. Am. Chem. Soc. 143, 891–901.

Biederer, T., Cao, X., Südhof, T.C., Liu, X., 2002. Regulation of APP-dependent transcription complexes by Mint/X11s: differential functions of Mint isoforms. J. Neurosci. 22 (17), 7340–7351.

Caster, A.H., Kahn, R.A., 2013. Recruitment of the Mint3 adaptor is necessary for export of the amyloid precursor protein (APP) from the Golgi complex. J. Biol. Chem. 288 (40), 28567–28580.

Chaufty, J., Sullivan, S.E., Ho, A., 2012. Intracellular amyloid precursor protein sorting and amyloid-beta secretion are regulated by Src-mediated phosphorylation of Mint2. J. Neurosci. 32, 9613–9625.

Cirrito, J.R., Kang, J.E., Lee, J., Stewart, F.R., Verges, D.K., Silverio, L.M., Bu, G., Mennerick, S., Holtzman, D.M., 2008. Endocytosis is required for synaptic activity-dependent release of amyloid-beta in vivo. Neuron 58, 42–51.

Dal Canto, M.C., 1996. The Golgi apparatus and the pathogenesis of Alzheimer's disease. Am. J. Pathol. 148, 355–360.

Das, U., Scott, D.A., Ganguly, A., Koo, E.H., Tang, Y., Roy, S., 2013. Activity-induced convergence of APP and BACE-1 in acidic microdomains via an endocytosis-dependent pathway. Neuron 79, 447–460.

Fourriere, L., Gleeson, P.A., 2021. Amyloid beta production along the neuronal secretory pathway: Dangerous liaisons in the Golgi? Traffic 22, 319–327.

Gross, G.G., Lone, G.M., Leung, L.K., Hartenstein, V., Guo, M., 2013. X11/Mint genes control polarized localization of axonal membrane proteins in vivo. J. Neurosci. 33 (19), 8575–8586.

Haass, C., Kaether, C., Thinakaran, G., Sisodia, S., 2012. Trafficking and proteolytic processing of APP. Cold Spring Harb. Perspect. Med. 2 (5), a006270.

Ho, A., Liu, X., Südhof, T.C., 2008. Deletion of Mint proteins decreases amyloid production in transgenic mouse models of Alzheimer's disease. J. Neurosci. 28 (53), 14392–14400.

Jensen, T.M.T., Albertsen, L., Bartling, C.R.O., Haugaard-Kedström, L.M., Strømgaard, K., 2018. Probing the Mint2 Protein-Protein Interaction Network Relevant to the Pathophysiology of Alzheimer's Disease. Chembiochem 19 (11), 1119–1122.

Lai, A., Sisodia, S.S., Trowbridge, I.S., 1995. Characterization of sorting signals in the beta-amyloid precursor protein cytoplasmic domain. J. Biol. Chem. 270, 3565–3573.

Makhoul, C., Gosavi, P., Gleeson, P.A., 2019. Golgi Dynamics: The Morphology of the Mammalian Golgi Apparatus in Health and Disease. Front. Cell Dev. Biol. 7, 112.

Matos, M.F., Xu, Y., Dulubova, I., Otwinowski, Z., Richardson, J.M., Tomchick, D.R., Rizo, J., Ho, A., 2012. Autoinhibition of Mint1 adaptor protein regulates amyloid precursor protein binding and processing. Proc. Natl. Acad. Sci. U. S. A. 109 (10), 3802–3807.

Okamoto, M., Südhof, T.C., 1997. Mints, Munc18-interacting proteins in synaptic vesicle exocytosis. J. Biol. Chem. 272 (50), 31459–31464.

Okamoto, M., Matsuyama, T., Sugita, M., 2000. Ultrastructural localization of mint1 at synapses in mouse hippocampus. Eur. J. Neurosci. 12 (8), 3067–3072.

Perez, R.G., Soriano, S., Hayes, J.D., Ostaszewski, B., Xia, W., Selkoe, D.J., Chen, X., Stokin, G.B., Koo, E.H., 1999. Mutagenesis identifies new signals for beta-amyloid precursor protein endocytosis, turnover, and the generation of secreted fragments, including Abeta42. J. Biol. Chem. 274, 18851–18856.

Selkoe, D.J., Hardy, J., 2016. The amyloid hypothesis of Alzheimer's disease at 25 years. EMBO Mol. Med. 8, 595–608.

Stieber, A., Mourelatos, Z., Gonatas, N.K., 1996. In Alzheimer's disease the Golgi apparatus of a population of neurons without neurofibrillary tangles is fragmented and atrophic. Am. J. Pathol. 148, 415–426.

Sullivan, S.E., Dillon, G.M., Sullivan, J.M., Ho, A., 2014. Mint proteins are required for synaptic activity-dependent amyloid precursor protein (APP) trafficking and amyloid beta generation. J. Biol. Chem. 289, 15374–15383.